Energy distributions in multiple photon absorption experiments

K. Mehlig, K. Hansen,[a] M. Hedén, A. Lassesson,[b] A. V. Bulgakov,[c] and E. E. B. Campbell
Department of Experimental Physics, Göteborg University and Chalmers University of Technology, SE-41296 Göteborg, Sweden

(Received 4 November 2003; accepted 3 December 2003)

Photofragmentation experiments on molecules and clusters often involve multiple photon absorption. The distributions of the absorbed number of photons are frequently approximated by Poisson distributions. For realistic laser beam profiles, this approximation fails seriously due to the spatial variation of the mean number of absorbed photons across the laser beam. We calculate the distribution of absorbed energy for various laser and molecular-beam parameters. For a Gaussian laser beam, the spatially averaged distributions have a power-law behavior for low energy with a cutoff at an energy which is proportional to fluence. The power varies between -1 for an almost parallel laser beam and $-5/2$ for a divergent beam (on the scale of the molecular beam). We show that the experimental abundance spectra of fullerenes and small carbon clusters can be used to reconstruct the distribution of internal energy in the excited C_{60} molecule prior to fragmentation and find good agreement with the calculated curves. © *2004 American Institute of Physics.*
[DOI: 10.1063/1.1643896]

I. INTRODUCTION

A large amount of information on clusters and molecules has been gathered in experiments which involve photoexcitation and subsequent fragmentation or electron emission from the excited molecule.[1] A strong experimental motivation for the choice of photoexcitation over other means of excitation is the availability of lasers since they provide both very well-defined units of energy and very high fluxes of these. One drawback of the method arises in studies of statistical processes in molecules with large heat capacities, viz. the fact that several photons need to be absorbed to reach excitation energies where processes occur on experimentally accessible time scales. The absorption of 10 or 20 photons can very rarely be controlled to a degree that one can state with confidence that the species studied has absorbed a specific number of photons. Instead, the number of absorbed photons is described by a distribution of finite width. In connection with statistical processes, the photon number distribution must be considered wide if the relevant (energy dependent) rate constant changes significantly across the width of the energy distribution. Since rate constants depend strongly on internal excitation energy, this situation very often appears. As a consequence, decays observed in ensembles of molecules, which contain a significant range of different rate constants, appear to be nonexponential in time.

A result of the present work is that energy distributions generated by lasers are likely to be much broader than the Poisson distribution, which is frequently used, and peaked at the low-energy end. This is important for the conclusions to be drawn from the temporal behavior of certain reactions, e.g., from the $1/t$ (or $1/t^p$, $p<1$) behavior observed in the decay or production rate of fullerene anions[2] or cations,[3] respectively. Experimentally, a decay of this kind has been observed to be robust to changes in laser fluence, in disagreement with the predictions one obtains using Poisson distributions in energy.[4]

It is also important in connection with mass distributions produced or influenced by fragmentation processes. An example, which will be examined here, is the distribution of fullerenes and small carbon clusters produced in the photofragmentation of C_{60}. The decay rates, which are generally assumed to describe the process of subsequent C_2 emission, are of thermal origin and thus very sensitive to the energy content of the respective parent molecule. The amount of fragmentation, i.e., the number of lost carbon units, mainly reflects the excitation energy initially deposited in the C_{60} and the size-to-size variation in dissociation energies of the respective parent molecule.[5] Since the dissociation energies for fullerenes smaller than C_{60} as well as C_{60} itself are rather well known, the measured fragment ion abundancies can serve as a testing ground for the internal energy distributions to be derived.

The effect of a Gaussian laser beam profile on the ionization yield following multiphoton absorption in gases of atoms has been investigated earlier.[6,7] It was shown that at high enough laser fluences, the increase of ion yield with fluence is determined by the increase of the interaction volume between the laser beam and gas. This work differs from the present one in two aspects. First, we calculate the whole energy distribution due to multiple photon absorption, and not just the amount exceeding the ionization threshold in a multiphoton process. Second, we consider the combined effect of a Gaussian laser beam and a molecular beam of finite size.

[a]Electronic mail: klavs@fy.chalmers.se
[b]Present address: Institute of Physik, Ernst-Moritz-Arndt Universität Greifswald, D-17487 Greifswald, Germany.
[c]Permanent address: Institute of Thermophysics, Prospect Lavrentyev 1, RU-630090 Novosibirsk, Russia.

The article is organized as follows: In Sec. II, we calculate the internal energy distribution of particles in a molecular beam due to the sequential absorption of photons from a Gaussian beam. Section III describes how the fragmentation products of highly excited C_{60} are measured, and Sec. IV A describes how they are used to obtain the initial internal energy distribution. Section IV B is devoted to the comparison between theoretical and experimental results followed by a critical discussion of energy loss channels other than sequential C_2 loss (Sec. IV C). The special case of C_4 loss is treated in the Appendix.

II. MULTIPLE PHOTON ABSORPTION IN MOLECULAR-BEAM EXPERIMENTS

The energy content of a molecule in a beam subject to laser radiation is a sum of the thermal energy from the source, the energy of the photons absorbed, and the energy released in connection with ionization, fragmentation, and radiation. For laser pulse durations of nanoseconds or longer, i.e., long compared to the electron–phonon coupling time,[8] the absorbed energy can be assumed to be equally distributed among the vibrational degrees of freedom of the molecule. The only exception seems to be the lowest lying triplet state, with a lifetime of 1 μs at 7 eV vibrational energy content. Its influence can be neglected, however, because the electronic energy involved is low (1.7 eV) and the lifetime is exponentially small for excitation energies needed to induce the long decay chains of interest here.[9] This allows for a description in terms of thermal processes, which depend on the internal energy of the molecule only and not on the details of the excitation process.

The situation is described by a distribution of internal energies rather than a specific value, not only due to the statistical nature of the absorption process but also due to the fact that each molecule experiences a different value of laser fluence depending on its position within the beam. The dependence of the internal energy distribution of the ensemble of molecules on the particular experimental conditions used in the photoabsorption experiment, such as the spatial profile of the laser fluence and the spatial distribution of the molecular beam, is the main subject of our study. Since we will not consider the detailed mechanism of the excitation processes leading to a certain internal energy, we use an average value for the photoabsorption cross section.

With a constant photoabsorption cross section, σ, the probability of absorbing n photons with photon energy E_{ph} and a specific value of laser fluence F, is given by the Poisson distribution with parameter $\lambda=\sigma F/E_{\mathrm{ph}}$:

$$P_n=e^{-\lambda}\frac{\lambda^n}{n!}. \tag{1}$$

In the following, we assume that the laser profile has a Gaussian shape, characteristic of the lowest-order transverse mode. Initially, we also assume that the variation of the laser beam width along the axis can be neglected (parallel beam) and that the molecular density is homogeneous across the laser profile. These restrictions will be relaxed later. Then, λ varies as

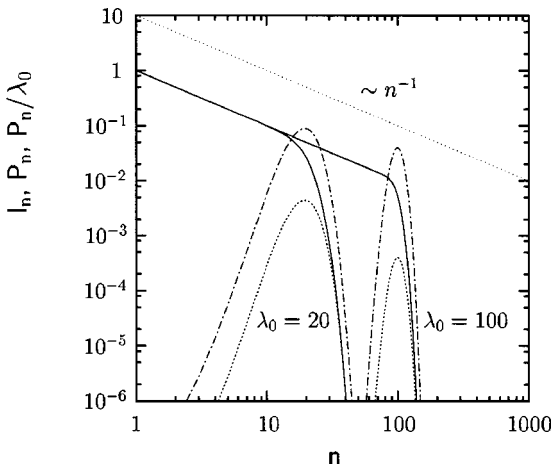

FIG. 1. The Poisson distribution averaged across a Gaussian laser beam profile, I_n, as given by Eq. (4) (solid lines), compared to the Poisson distribution with constant parameter λ_0 [Eq. (1)] (dot–dashed lines). Both distributions are normalized to equal amount of average absorbed energy ($=\lambda_0 E_{ph}$). For $n\ll\lambda_0$, we have $I_n\sim n^{-1}$ as expected from Eq. (5). The n dependence beyond the cutoff is best described by the Poisson distribution P_n/λ_0 (dotted line), i.e., by the fraction of molecules, which see the maximal laser fluence in the center of the beam.

$$\lambda(r)=\lambda_0 e^{-2r^2/w_0^2}, \tag{2}$$

with r denoting the radial distance from the center of the beam. The two parameters here are the maximum value of the fluence, through $\lambda_0=\sigma F_0/E_{ph}$, and the laser beam width, w_0.

The total amount of molecules that absorb n photons is given by

$$I_n\propto\int_0^\infty dr r P_n=\int_0^\infty dr r e^{-\lambda(r)}\frac{\lambda(r)^n}{n!}, \tag{3}$$

where a factor related to the density of the molecules has been left out. Inserting Eq. (2) and using the substitution $u=\lambda(r)$ gives

$$I_n\propto\int_0^{\lambda_0} du\,\frac{e^{-u}u^{n-1}}{n!}. \tag{4}$$

The limit at high fluences, $\lambda_0\to\infty$, is

$$I_n\propto\int_0^\infty du\,\frac{e^{-u}u^{n-1}}{n!}=\frac{1}{n}. \tag{5}$$

At lower fluences, I_n is proportional to n^{-1} up to a cutoff at λ_0. At this point, the function begins to drop off and at higher values of n has a dependence which roughly follows the Poisson distribution with parameter λ_0 (Fig. 1).

The above result does not take into account the finite size and shape of the molecular beam or the fact that the shape of a laser beam changes along the line of propagation. Often, molecular and laser beams cross each other perpendicularly. We will treat this configuration in detail here. In the case of a narrow laser beam of sufficiently low divergence, i.e., where the laser beam waist is always small compared to the extension of the molecular beam, we may proceed as follows: Along the direction of the laser beam, which

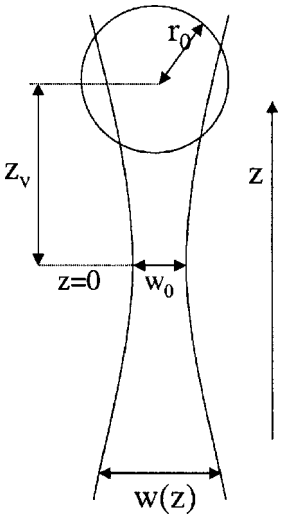

FIG. 2. Geometry of the interaction region between laser beam (along the z axis) and molecular beam (circle) crossing at right angles. The laser beam waist increases with the distance from the focus at $z=0$, cf. Eq. (6). If the narrow-beam approximation is valid, we can neglect the variation of molecular density perpendicular to the laser beam.

is taken as the z axis, we add up contributions of the form (4), with the laser beam waist and peak fluence now being z dependent, i.e.,

$$w(z)=w_0\sqrt{1+\frac{z^2}{z_0^2}},\quad F_0(z)=F_0(0)\frac{w_0^2}{w(z)^2}. \tag{6}$$

The Rayleigh length, z_0, is a measure of the inverse divergence of the laser beam and $F_0(0)$ is the fluence at the focal point $z=0$. Each term of the sum is weighted with the density of the molecular beam at the particular value of z, i.e.,

$$I_{\mathrm{mol}}(z)\propto\exp\left(-\frac{(z-z_v)^2}{2r_0^2}\right), \tag{7}$$

where z_v denotes the distance between the center of the molecular beam and the laser focus and r_0 denotes the radius of the molecular beam, cf. Fig. 2. Hence, the expression corresponding to Eq. (3) reads

$$I_n(\mathrm{total})\propto\int_{-\infty}^{\infty}dz e^{-(z-z_v)^2/2r_0^2}\int_0^{\infty}rdr\frac{\lambda(r,z)^n}{n!}e^{-\lambda(r,z)}, \tag{8}$$

with $\lambda(r,z)=\lambda_0 w_0^2/w(z)^2\exp[-2r^2/w(z)^2]$ and $\lambda_0=\sigma F_0(0)/E_{ph}$. Transforming to $u=\lambda(r,z)$ yields

$$I_n(\mathrm{total})\propto\int_{-\infty}^{\infty}dz w(z)^2 e^{-(z-z_v)^2/2r_0^2}\int_0^{\lambda_0 w_0^2/w(z)^2}\times du\frac{e^{-u}u^{n-1}}{n!}. \tag{9}$$

A change of variable to $x\equiv z/z_0$ ($x_v\equiv z_v/z_0$) gives

$$I_n(\mathrm{total})\propto z_0\int_{-\infty}^{\infty}dx(1+x^2)e^{-(x-x_v)^2z_0^2/2r_0^2}\times\int_0^{\lambda_0/(1+x_v^2)}du\frac{e^{-u}u^{n-1}}{n!}. \tag{10}$$

In the following, we consider two limiting cases, where the parameter z_0/r_0 is either small or large compared to unity.

The case where $(z_0/r_0)^2\gg 1$ corresponds to a laser beam with very small divergence. In this case, the Gaussian integral in Eq. (10) restricts the value of x to values very close to x_v. With $x=x_v$ in the upper limit of the second integral, we obtain to lowest order in r_0/z_0,

$$I_n(\mathrm{total})\propto\sqrt{2\pi}r_0(1+x_v^2)\int_0^{\lambda_0 1/1+x_v^2}du\frac{e^{-u}u^{n-1}}{n!},\quad 1\ll(z_0/r_0)^2. \tag{11}$$

For n sufficiently small, we get

$$I_n(\mathrm{total})\propto\sqrt{2\pi}r_0(1+x_v^2)\frac{1}{n},\quad 1\ll(z_0/r_0)^2,\quad n\ll\frac{\lambda_0}{1+x_v^2}. \tag{12}$$

The distribution of absorbed photons with the expectation value $\lambda(r,z)$ averaged along a weakly divergent laser beam is thus identical to the average over a single cross section as given by Eq. (4), except that the highest absorbed photon number is reduced depending on the position of the laser focus relative to the molecular beam, while the amplitude for the lower photon numbers is increased accordingly, thus accounting for energy conservation.

In the other limit, $(z_0/r_0)^2\ll 1$, we approximate the u integral in Eq. (10) with a function which is $1/n$ for $n<\lambda_0/(1+x^2)$ and zero otherwise. For n fixed, the upper limit of the remaining integral is then given by $x=\sqrt{\lambda_0/n-1}$. The Gaussian in the x integral may be set to unity. A better approximation is obtained if we instead insert the value of x at the upper limit. Hence,

$$I_n(\mathrm{total})\propto 2z_0 e^{-(\sqrt{\lambda_0/n-1}z_0/r_0-z_v/r_0)^2/2}\times\int_0^{\sqrt{\lambda_0/n-1}}dx(1+x^2)\frac{1}{n}$$
$$\propto\frac{2z_0}{3}e^{-(\sqrt{\lambda_0/n-1}z_0/r_0-z_v/r_0)^2/2}\times\frac{1}{n}\left(\frac{\lambda_0}{n}-1\right)^{1/2}\left(2+\frac{\lambda_0}{n}\right),\quad (z_0/r_0)^2\ll 1. \tag{13}$$

For intermediate values of n, this reduces to

$$I_n(\mathrm{total})\propto\frac{2z_0}{3}e^{-z_v^2/2r_0^2}\lambda_0^{3/2}n^{-5/2},\quad (z_0/r_0)^2\ll 1,\quad 1\ll n\ll\lambda_0. \tag{14}$$

It should be noted that the validity of the narrow-beam approximation requires that the laser beam waist at the edge of the molecular beam is still small compared with the extension of the molecular beam, i.e.,

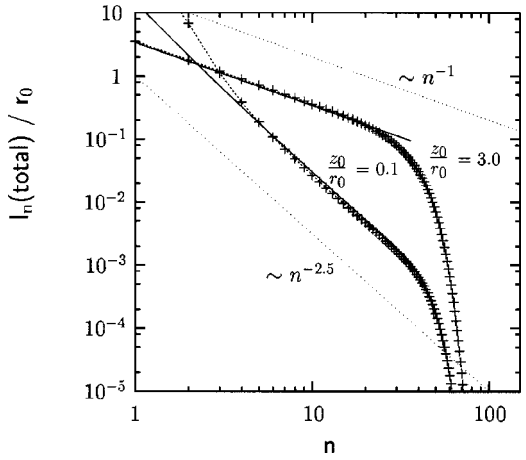

FIG. 3. The probability to absorb n photons, averaged over the interaction volume between laser and molecular beam, as given by Eq. (10), for $\lambda_0 = 50$ and two different focusing conditions, $z_0/r_0 = 3.0$ and 0.1 (crosses, dotted line). The geometry as described by the distance between laser focus and molecular beam, z_v, and the extension of the C_{60} beam, r_0, is kept constant, $z_v/r_0 = 1.7$; thus $x_v = z_v/z_0 = 0.6$ and 17, respectively. The approximations as given by Eqs. (12) and (13) are shown as solid lines.

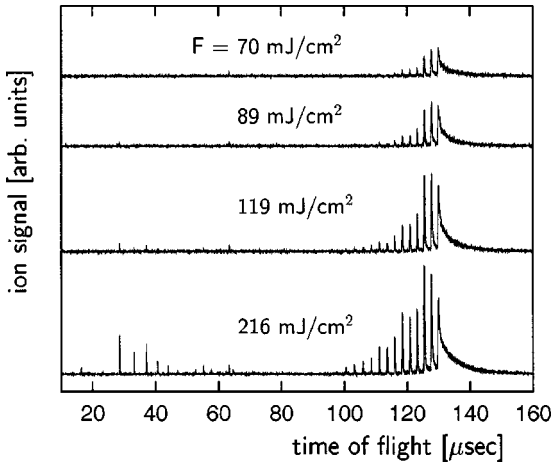

FIG. 4. Measured (fragment) ion intensities as obtained from the RETOF mass spectrometer after multiple photon excitation of gas phase C_{60}. As the laser fluence increases, fragments down to C_{32}^+ are observed, which still preserve the cagelike structure. While the relative yield of fullerene fragments saturates at higher fluence values, small fragments appear at around $F_{sf} \sim 100$ mJ/cm^2. The small peak at 63 μs is due to pump oil.

$$r_0 \gg w|_{z_v + r_0} \approx w_0 \frac{z_v + r_0}{z_0}. \tag{15}$$

Figure 3 summarizes the results for a Poisson distribution averaged along a Gaussian laser beam, which is crossed by a molecular beam. The calculations, which are done within the narrow-beam approximation using Eq. (10), are shown for two limiting cases, namely for an almost parallel laser beam (on the scale of the molecular beam), $z_0/r_0 = 3.0$, and for a situation, where the laser beam is more strongly focused, $z_0/r_0 = 0.1$. The approximations for large and small values for z_0/r_0, Eqs. (12) and (13), are shown as well. The crossover from a n^{-1} to a $n^{-2.5}$ dependence is clearly visible. For a laser beam of low divergence, we obtain a broad energy distribution $I_n \sim n^{-1}$ as in the case of one single cross section, cf. Eq. (5). In the other case, only the (small) fraction of molecules in the focal region of the laser can absorb λ_0 photons or more, which leads to the steeper decrease, $I_n \sim n^{-2.5}$. In the weakly divergent case, the number of molecules absorbing a specific number of photons, $n_0 (\ll \lambda_0/(1+x_v^2))$, stays constant, if the fluence is increased. This is in contrast to the strongly divergent case, where the fluence dependence ($\sim \lambda_0^{3/2}$) reflects the increase of interaction volume between the molecular and the laser beam.[7]

III. EXPERIMENTAL SETUP

The characteristic fragmentation pattern of highly excited C_{60} molecules may be used to reconstruct the internal energy distribution following photoabsorption, which can then be compared to the expressions calculated above. To this end, we will describe the photoabsorption experiments done with C_{60} in this section, and the further processing of the data in Sec. IV A.

Briefly, the experimental setup consists of a vacuum chamber, where the beam of C_{60} molecules is produced and excited with a laser, and a time-of-flight mass spectrometer equipped with a reflectron [reflectron time of flight (RETOF)]. The C_{60} powder (99.5% purity) is sublimed in a resistively heated oven at 400–500 °C, placed immediately below the acceleration stage of the RETOF. We use a 4 ns, 100 μJ, N_2 laser with photon energy 3.68 eV (337 nm). This photon energy is a factor of two to three times smaller than typical dissociation and ionization energies for the fullerenes involved. The laser beam is oriented at right angles with respect to the molecular beam as well as to the extraction fields for the RETOF. After ionization and fragmentation the ions are accelerated to energies of several keV and fly in the first fieldfree region for tens of μs before entering the reflectron, after which they fly freely for about a meter and are detected by a dual-channelplate detector. The ion signal is recorded with an oscilloscope.

Laser fluences are measured with a calorimeter and refer to values averaged over several seconds. The shot-to-shot fluctuations in the laser were 10%–15%. The laser was focused with a 300 mm lens to a beamspot of $w_0 \leqslant 50$ μm. The intensity profile perpendicular to the beam axis was measured by moving a pinhole attached to the calorimeter across the laser spot, for several values of z_v. The beam divergence, $\alpha = w_0/z_0$, was found to be 0.011 radians, corresponding to a Rayleigh length of $z_0 = 4.5$ mm. Figure 4 gives an example of ion spectra recorded at different values of laser fluence.

The profile of the molecular beam was obtained by subliming C_{60} onto glass plates in the ionization chamber. Absorption spectra of the films were recorded at different points on the glass plates using an ultraviolet-visible (UV-VIS) spectrometer. The intensity of the absorption peak around 430–450 nm was used as a measure of film thickness. The beam profile fitted Eq. (7) well and gave $r_0 = 12.9$ mm. The experimental data reported here were taken with the laser focus located at $z_v = 22$ mm before the center of the molecular beam, well within the limit of the narrow-beam approximation $w(z) \ll r_0$ for $|z - z_v| \leqslant r_0$.

IV. RESULTS AND COMPARISON WITH THEORY

A. Distribution of internal energy of photoexcited C_{60} from fragment ion abundancies

To convert the integrated measured fragment ion intensities into a distribution of inital internal energy of C_{60}, we assume that the fragment ions are produced from C_{60}^+ by subsequent emission of neutral C_2 units and that the abundancy of a particular fragment is proportional to the integral of the energy distribution over the energy interval from which it is created. Let D_N denote the dissociation energy of the (fragment) ion C_N^+ with respect to C_2 emission and $c_N = 3N-7$ the microcanonical heat capacity (we use $k_B=1$ in the following). Consider the step $N \rightarrow N-2$. Dissociation will occur as long as the dissociation rate exceeds the inverse of the typical measurement time t, which is of the order of microseconds. The rate constant can, to a good approximation, be written in a simple Arrhenius-type form:[5]

$$k_N(E) = \omega_N e^{-D_N/T_e(E)}, \tag{16}$$

where the emission temperature is given by $T_e(E)=(E+E_0-D_N/2)/c_N$, for temperatures high compared with the vibrational quanta of the molecule. E_0 is equal to the sum of zero-point energies of the vibrational motion of the harmonic oscillators [which enters both the canonical and the microcanonical $E(T)$ relation at high temperatures], the thermal energy from the oven and the ionization potential of C_{60} ($=7.6$ eV). With an effective energy $E' \equiv E+E_0-D_N/2$, one has, for the upper limit on the internal energy which can be stored in the C_N^+ fragment,

$$E' = \frac{D_N c_N}{G}, \tag{17}$$

where G is the Gspann parameter, $G=D_N/T_e$ and T_e is the emission temperature which gives a rate constant of $1/t$. We will use an average value of $G=\ln(\omega_N t)=33$ (Refs. 10 and 11) for the fullerenes with $N<60$. This corresponds to a frequency factor of $\omega = 2\times 10^{19}\,\mathrm{s}^{-1}$. The value for C_{60} may be higher, but this is taken into account by using the measured appearance energy of C_{58}^+ instead (see below).

Since every emission step reduces the internal energy by the respective dissociation energy, the lower limit of internal energy in C_{60}^+ for creation of C_{N-2}^+ is given by

$$E_{N-2}^{\min} = \frac{D_N c_N}{G} + \sum_{i=N+2}^{60} D_i\,. \tag{18}$$

The upper limit is identical to the lower limit for creation of C_{N-4}^+, i.e. $E_{N-2}^{\max}=E_{N-4}^{\min}$. This mapping of energy distributions on fragment sizes assumes that there is a limiting energy, above which a certain reaction will occur and below which it is suppressed. It is a good approximation for clusters where $c_N \ll G^2$.[12] The yield of the $(N-2)$th fragment ion is proportional to the width of the interval $E_{N-2}^{\max}-E_{N-2}^{\min}$ times the internal energy distribution $\rho(E)$, averaged over this interval,[5]

$$Y_{N-2} \propto \left(D_N - \frac{D_N c_N - D_{N-2} c_{N-2}}{G} \right) \rho(E). \tag{19}$$

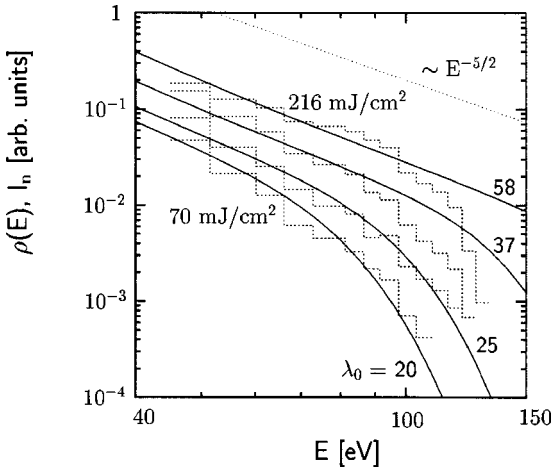

FIG. 5. Internal energy distributions for photoexcited C_{60} as obtained from the measured fragment ion intensities shown in Fig. 4 according to Eq. (19) (dashed line), in comparison with calculated distributions (solid line). For the latter, the averaged absorption probability I_n [cf. Eq. (10)] has been plotted vs the internal energy $E_n = E_{\mathrm{th}} + nE_{\mathrm{ph}}$, with $E_{\mathrm{th}} \sim 4$ eV for $T = 723$ K and $E_{\mathrm{ph}} = 3.68$ eV. The experimental fluence increases from left- to right-hand side, the values are the same as given in Fig. 4. Note that λ_0 is related to the fluence at the focus of the laser beam, which is different from the center of the molecular beam in the experiment considered here.

The energy interval covered by one cluster size corresponds to approximately one dissociation energy, or two to three photons in our case. The difference between the effective energy and the excitation energy is very small when only energy *intervals* such as $E_{N-2}^{\max}-E_{N-2}^{\min}$ are considered, because the offset term $E_0-D_N/2$ is fairly constant for C_2 emission from $N=44-60$. Dividing the integrated fragment ion intensities Y_N, measured in the time-of-flight (TOF) spectrum, by the width of the energy interval over which they are created, allows us to obtain a piecewise constant approximation to the original distribution of internal energy in C_{60}^+.

We used the dissociation energies measured by Tomita *et al.*[13] for fullerene cations down to C_{48} and extrapolated the latter value to the smaller fullerene fragments. The resulting energy distribution did not significantly depend on the precise values of the dissociation energies. We used the appearance energy of $E_{58}^{\min}=45$ eV for C_{58}^+, which is measured in electron impact ionization experiments.[14] The finite heat bath correction $D/2$ and the offset E_0 are automatically included in the appearance energy.

B. Comparison with calculated internal energy distributions

Figure 5 shows energy distributions, which are derived from the mass spectra shown in Fig. 4, obtained at different laser fluences. They were recorded with the parameters $z_v/r_0=1.7$ and $z_0/r_0=0.35$. The abundance maxima due to local stability (at $N=50$, for instance) have disappeared as expected from Eq. (19).

Sufficiently below the high-energy cutoff, we find a dependence $\sim E^{-2.5}$ as expected for these focusing conditions, cf. Eq. (14). In this region, the experimental energy distributions are well described by the calculated curves obtained

from Eq. (10), with λ_0 increasing linearly with the measured fluence. Around the cutoff itself, the experimentally determined energy distributions for the two highest values of laser fluence fall off more rapidly than the calculated ones, which we attribute to the opening of another reaction channel, namely the production of small fragments. These are associated with an opening and destruction of the fullerene cage structure and most likely a reduction of the dissociation energy (compared to multiple C_2 loss) as well as a release of potential energy.

As a consequence of the broad energy distribution derived from Eqs. (10)–(14), the intensity ratio of a particular fragment ion relative to its precursers saturates, while the absolute yield increases with fluence according to Eqs. (13) and (14). This observation is in contrast to, e.g., the collision experiments described in Ref. 15, where the appearance and peak energies of each fragment size are well separated in collision energy.

As the relative yield of the largest fullerene fragments starts to saturate (at approximately $F_{sf}=100\,\mathrm{mJ/cm^2}$), there is an increase of small fragments indicating that the most highly excited C_{60} decay into non-fullerene type fragments. Since this process does not happen via stepwise C_2 loss, the abundance of small fragments does not give information on $\rho(E)$ directly. But if we assume that C_{60} molecules with energy higher than a critical energy E_{sf} will decay into small fragments, the theoretically predicted high-energy tail of $\rho(E)$ can be numerically integrated and compared with the total yield of small fragments, Y_{sf}:

$$Y_{sf} \propto \int_{E_{sf}}^{\infty} dE\rho(E) \propto \int_{\lambda_{sf}}^{\infty} dn I_n(\mathrm{total}), \tag{20}$$

where $I_n(\mathrm{total})$ depends on λ_0 as given by Eq. (10). From the deviation between the measured and calculated internal energy distributions, we obtain a critical energy for small fragment production, which is given by $E_{sf}=(110\pm10)$ eV. The average photoabsorption cross section is thus given by $\sigma=E_{sf}/F_{sf}=1.8\,\mathrm{Å}^2$, which is in accordance with values given in literature for a wavelength of 337 nm (Ref. 16) and with the value of 1.9 $\mathrm{Å}^2$ recently estimated from the comparison of the fragmentation of C_{60}^+ and $La@C_{82}^+$ with a maximum entropy model.[17] Figure 6 shows good agreement between the measured and calculated yield of small fragments. The latter does not depend crucially on the precise value of σ (or E_{sf}) due to the following scaling property of the asymptotic solution: If we calculate Y_{sf} using Eq. (14), we see that

$$Y_{sf} \propto \lambda_0^{3/2} \int_{\lambda_{sf}}^{\lambda_0} \frac{1}{n^{5/2}} dn = \frac{2}{3}\left(\left(\frac{\lambda_0}{\lambda_{sf}}\right)^{3/2} - 1\right)$$
$$\propto \left(\frac{F_0(0)}{F_{sf}}\right)^{3/2} - 1, \quad F_0(0) \gg F_{sf}, \tag{21}$$

which does not depend on σ.

Muigg *et al.*[18] measured an appearance energy of (85 ± 5) eV for the onset of production of small fragments. The critical energy used here differs from the onset energy, which depends on statistics, and renders a direct comparison difficult. One expects, however, that the appearance energy is less than the critical energy, as observed.

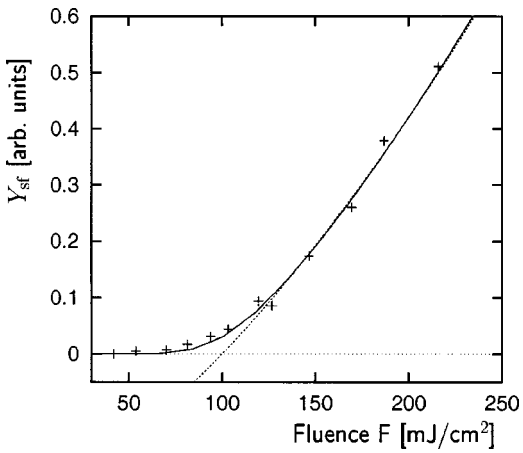

FIG. 6. Fluence dependence of the yield of small fragments. The experimental data points are well described by the calculated curve obtained from Eq. (20) with $E_{sf}=110$ eV (solid line). The asymptotic behavior according to Eq. (21) is shown as well (dashed line).

C. Competing channels and other energy loss terms

In addition to the emission of C_2, the fullerene cations can emit larger neutral fragments, such as C_3 and C_4. If these channels were important, they would of course influence the abundance spectrum and invalidate the energy distributions derived from that. For the positively charged fullerenes, only even numbered fragments are observed and the main channel competing with C_2 emission is C_4 loss.

There are several reports of experimental evidence for C_4 emission from fullerenes. Some pertain to collision experiments, where the energy transfer is much more rapid than the ns time scale relevant here.[19] They are, therefore, not of direct relevance here. C_4 has also been detected by the postionization of the neutral fragments after the laser excitation of C_{60}.[20] It is, however, not obvious whether these molecules appear because of C_4 emission from fullerenes or if they are the final product of a longer decay chain. More direct evidence is found in the metastable decay in RETOF mass spectrometers, such as the one used in this work, where C_4 emission is not observed. Unfortunately, these experiments are only sensitive to time scales of 100 ns and up, and one has to rely on a theoretical estimate to give limits for the much faster processes that are relevant here. This estimate can be found in the Appendix.

A major uncertainty in relating fragment ion abundancies to distributions of internal energy is the presence of the neutral decay channel: Neutral C_{60} is known to emit both electrons and dimers in competition, and the neutral fragmentation channel is the dominant one,[21] accounting for about 97% of the decays at high energies. There will, therefore, be a large component of neutral fragments which can potentially undergo delayed ionization and add abundance to the fragment ion intensities. Indeed, delayed ionization of fullerene fragments has recently been observed in coincidence experiments,[11] mainly from C_{58}, C_{56}, and C_{50}.

The effect is most serious for low ionization potentials and high dissociation energies, where the branching to ionization is highest. With the measured values of ionization and dissociation energies,[22,13] the lowest IE/D ratio is found for C_{60}. The 3% ionization yield reported in Ref. 21 would seem to rule out any significant contribution from ionization at lower masses. There are, however, special effects inherent to C_{60}, which tend to enhance the neutral fragmentation relative to ionization and which are not present for the fullerenes of lower mass, such as the high electronic degeneracy of C_{58} relative to the one for C_{60} or, more generally, the larger partition function for the valence electrons. This will, by detailed balance arguments, increase the evaporative rate constant for C_2 emission. Another effect is the presumably larger number of thermally accessible isomers of C_{58} compared with C_{60}.

A related problem is that neutral fragments, which are created during the laser pulse, can get directly ionized by additional photons from the same pulse. This may have an influence on the observed abundancies; the more, the higher the laser fluence. However, experiments with postionization of neutral fragments have shown that neutral and ionic fragments have similar distributions.[23] This suggests that ionization of fragments, direct or delayed, does not have a major effect on the relative yield of fullerene fragment ions.

V. CONCLUSION

The distribution of energy absorbed by a molecular beam exposed to a perpendicular laser beam with a Gaussian profile has been calculated for a number of different laser and molecular-beam parameters. For a laser beam which is narrow compared to the extension of the molecular beam, the number of absorbed photons varies as a power law up to a well-defined cutoff. The exponent describing the distribution depends on the specific geometry and varies between -1 and $-5/2$. A comparison with experimental energy distributions, derived from abundance spectra of fullerene fragment ions, shows good agreement with the calculations.

ACKNOWLEDGMENTS

This work was supported by the EU Cluster Cooling Network (HPRN-CT-2000-00026). The authors thank Andrej Gromov for help with the UV-VIS spectrometer.

APPENDIX: IMPORTANCE OF C_4 LOSS

A simple estimate of the importance of C_4 emission relative to C_2 emission can be made as follows: Let R denote the ratio of thermal emission rates for the two processes, i.e.,

$$R=\frac{\omega_4}{\omega_2}\exp\left(-\frac{D_{N,4}}{T-\frac{D_{N,4}}{2c_N}}+\frac{D_{N,2}}{T-\frac{D_{N,2}}{2c_N}}\right),$$

where the exponential form of Eq. (16) has been used for the rate constants. $D_{N,M}$ is the dissociation energy of the fragment ion C_N^+ with respect to loss of a neutral fragment of size M. The notation D_N used in the main text corresponds to $D_{N,2}$ here. T is the microcanonical temperature of the molecules before fragmentation, which for C_{60} is close to 4000 K at 1 μs,[24] and the microcanonical heat capacity is given by $c_N=3N-7$.

Using the abbreviation $T_e=T-D_{N,2}/2c_N$ for the emission temperature for C_2 emission, we may expand the exponent in the above expression as follows

$$-\frac{D_{N,4}}{T-\frac{D_{N,4}}{2c_N}}+\frac{D_{N,2}}{T_e}\approx-\frac{D_{N,4}-D_{N,2}}{T_e}\left(1+\frac{D_{N,4}}{2c_NT_e}\right)$$

$$=-\frac{D_{N,4}-D_{N,2}}{D_{N,2}}G\left(1+\frac{D_{N,4}}{2c_NT_e}\right),$$

where we used a Gspann parameter $G=D_{N,2}/T_e$ which is independent of fragment size.

To obtain an estimate for the ratio of pre-exponential factors, we assume that the C_4 molecule is linear in the ground state[25] and that the bondlengths are similar to those of C_2. This gives a factor of 10 on the rotational partition function of C_4 relative to the one for C_2 and a factor of 2 on the corresponding translational partition function.[26] Hence,

$$\frac{\omega_4}{\omega_2}\approx 20\frac{\sigma_{4,N-4}}{\sigma_{2,N-2}}, \tag{A1}$$

where the σ's are the capture cross sections for the processes indicated by the subscripts. The branching ratio is now given by

$$R\leqslant 20\frac{\sigma_{4,N-4}}{\sigma_{2,N-2}}\exp\left(-\frac{D_{N,4}-D_{N,2}}{D_{N,2}}G\left(1+\frac{D_{N,4}}{2c_vT_e}\right)\right).$$

The adiabatic value of $D_{N,4}$ can be estimated from a Born–Haber cycle as

$$D_{N,4}=D_{N,2}+D_{N-2,2}-D_{4,2},$$

where the dissociation energy of neutral C_4 is given by $D_{4,2}=7.3$ eV as found from the standard enthalpies of C_2 and C_4 formation from graphite. For fullerenes, we use the values given in Ref. 13. The values of $(D_{N,4}-D_{N,2})/D_{N,2}$ are then for $N=60$ through 50 equal to 0.09, 0.17, 0.13, 0.13, 0.17, and 0.11. With $G=33$ at the microsecond time scale, one gets branching ratios in the range

$$R=\frac{\sigma_{4,N-4}}{\sigma_{2,N-2}}\cdot(0.05\rightarrow 0.7).$$

Given the experimental evidence that C_4 emission from cationic fullerenes is below the detection limit on the μs time scale (cf. Sec. IV C), the calculated values of R imply a low attachment cross section for C_4 as compared to $\sigma_{2,N-2}$. One reason for this might be that C_4 attaches preferably as a bent molecule, which effectively increases the activation barrier of the process.

Whatever the explanation, we can set the μs branching ratio to a value below the detection threshold of a few percent and calculate an upper limit by extrapolating the Gspann parameter to shorter times;

$$G(t)=G(10\ \ \mu\text{s})+\ln\left(\frac{t}{10\ \ \mu\text{s}}\right).$$

A conservative estimate of the time t is to require that all atoms are emitted from C_{60} one by one during the laser pulse. This gives $t=170\,\mathrm{ps}$ and $G(t)=22$. Although the change in time is considerable, the branching ratio only changes by a factor of 4 on the average, and a factor of 7 at most. Combined with the low limit set by the experimental data for $G(10\,\mu\mathrm{s})=33$, we conclude that tetramer emission remains a minority channel, also at the highest excitation energies relevant here.

[1] See, e.g., E. E. B. Campbell and R. D. Levine, Annu. Rev. Phys. Chem. **51**, 65 (2000).
[2] K. Hansen, J. U. Andersen, P. Hvelplund, S. P. Møller, U. V. Pedersen, and V. V. Petrunin, Phys. Rev. Lett. **87**, 123401 (2001).
[3] K. Hansen and O. Echt, Phys. Rev. Lett. **78**, 2337 (1997).
[4] P. Stampfli and T. D. Märk, Phys. Rev. Lett. **82**, 459 (1999).
[5] K. Hansen and U. Näher, Phys. Rev. A **60**, 1240 (1999).
[6] I. N. Arutyunyan, G. A. Askaryan, and V. A. Pogosyan, JETP **31**, 548 (1970).
[7] M. R. Cervenan and N. R. Isenor, Opt. Commun. **13**, 175 (1974).
[8] K. Hansen, K. Hoffmann, and E. E. B. Campbell, J. Chem. Phys. **119**, 2513 (2003).
[9] R. Deng, M. Treat, O. Echt, and K. Hansen, J. Chem. Phys. **118**, 8563 (2003).
[10] K. Hansen and E. E. B. Campbell, J. Chem. Phys. **104**, 5012 (1996).
[11] S. Tomita, J. U. Andersen, K. Hansen, and P. Hvelplund, Chem. Phys. Lett. **382**, 120 (2003).
[12] U. Näher and K. Hansen, J. Chem. Phys. **101**, 5367 (1994).
[13] S. Tomita, J. U. Andersen, C. Gottrup, P. Hvelplund, and U. V. Pedersen, Phys. Rev. Lett. **87**, 073401 (2001).
[14] M. Foltin, M. Lezius, P. Scheier, and T. D. Märk, Chem. Phys. **98**, 9624 (1993).
[15] Y. Basir and S. L. Anderson, J. Chem. Phys. **107**, 8370 (1997).
[16] J. Berkowitz, *Atomic and Molecular Photoabsorption: Absolute Total Cross Sections* (Academic, San Diego, 2002), Chap. 6.8 and references therein.
[17] A. Lassesson, A. Gromov, K. Mehlig, A. Taninaka, H. Shinohara, and E. E. B. Campbell, J. Chem. Phys. **119**, 5591 (2003).
[18] D. Muigg, P. Scheier, K. Becker, and T. D. Märk, J. Phys. B **29**, 5193 (1996).
[19] R. Vandenbosch, B. P. Henry, C. Cooper, M. L. Gardel, J. F. Liang, and D. I. Will, Phys. Rev. Lett. **81**, 1821 (1998).
[20] K. R. Lykke, Phys. Rev. A **52**, 1354 (1995).
[21] R. Deng and O. Echt, J. Phys. Chem. A **102**, 2533 (1998).
[22] O. V. Boltanina, I. N. Ioffe, L. N. Siderov, G. Seifert, and K. Vietze, J. Am. Chem. Soc. **122**, 9745 (2000).
[23] K. R. Lykke and P. Wurz, J. Phys. Chem. **96**, 3191 (1992).
[24] F. Lépine, B. Climen, F. Pagliarulo, B. Baguenard, M. A. Lebeault, C. Bordas, and M. Hedén, Eur. Phys. J. D **24**, 393 (2003).
[25] M. T. Bowers, P. R. Kemper, G. von Helden, and P. A. M. van Koppen, Science **260**, 1446 (1993).
[26] We disregard the difference in the contribution of excited electronic states and the difference in vibrational frequencies of C_2 and C_4.